

Precise regulation of acid pretreatment for red mud SCR catalyst: Targeting on optimizing the acidity and reducibility

Xiang Zhang^{1*}, Yue Xuan^{1*}, Bin Wang¹, Chuan Gao¹, Shengli Niu¹, Gaiju Zhao⁴, Dong Wang (✉)^{1,2}, Junhua Li³, Chunmei Lu¹, John C. Crittenden²

¹ National Engineering Laboratory for Coal-Burning Pollutants Emission Reduction, School of Energy and Power Engineering, Shandong University, Jinan 250061, China

² School of Civil and Environmental Engineering and the Brook Byers Institute for Sustainable Systems, Georgia Institute of Technology, Atlanta, GA 30332, USA

³ State Key Joint Laboratory of Environment Simulation and Pollution Control, National Engineering Laboratory for Multi Flue Gas Pollution Control Technology and Equipment, School of Environment, Tsinghua University, Beijing 100084, China

⁴ Energy Institute, Qilu University of Technology (Shandong Academy of Sciences), Jinan 250013, China

HIGHLIGHTS

- The optimum SCR activity was realized by tuning the acid pretreatment.
- Optimized catalysts showed NO_x conversion above 90%.
- The NH₃ and NO adsorption capacity of Al-O₃-Fe is stronger than Fe-O₃-Fe.
- The formation of almandine consumes Fe³⁺ and Al³⁺ and weakens their interaction.

ARTICLE INFO

Article history:

Received 28 June 2021

Revised 15 October 2021

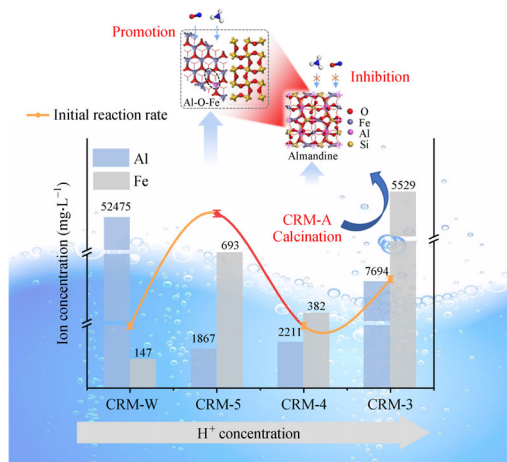
Accepted 20 October 2021

Available online 19 November 2021

Keywords:

Air pollution control
Nitrogen oxides
Selective catalytic reduction
Red mud
Solid waste utilization

GRAPHIC ABSTRACT



ABSTRACT

Red mud (RM), as an alkaline waste, was recently proved to be a promising substitute for the SCR catalyst. Dealkalization could improve the acidity and reducibility of red mud, which were critical for SCR reaction. However, the dealkalization effect depended on the reaction between acid solution and red mud. In this study, we realized the directional control of the chemical state of active sites through tuning the acid pretreatment (dealkalization) process. The pretreatment endpoint was controlled at pH values of 3–5 with diluted nitric acid. When the pH values of red mud were 3 and 5 (CRM-3 and CRM-5), activated catalysts showed NO_x conversion above 90% at 275°C–475°C. The high initial reaction rate, Ce³⁺/(Ce³⁺ + Ce⁴⁺) ratio, and surface acidity accounted for the excellent SCR performance of CRM-5 catalyst. Meanwhile, more Fe³⁺ on the CRM-3 surface improved the NH₃ adsorption. There was a strong interaction between Al and Fe in both CRM-5 and CRM-3 catalysts. DFT results showed that the adsorption capacity of the Al-O₃-Fe for NH₃ and NO is stronger than that of Fe-O₃-Fe, which enhanced the NO_x conversion of the catalyst. However, the almandine was formed in CRM-4, consumed part of Fe³⁺ and Al³⁺, and the interaction between Al and Fe was weakened. Also, deposited almandine on the catalyst surface covered the active sites, thus leading to lower NH₃-SCR activity.

© Higher Education Press 2022

✉ Corresponding author

E-mail: dwang473@gatech.edu

*These authors contributed equally to this work.

1 Introduction

Nitrogen oxides (NO_x), as severe urban pollutants, have adverse effects on human beings and the environment (Liu et al., 2019; Sun et al., 2019). The selective catalytic reduction with NH_3 (NH_3 -SCR) is the mainstream technology for controlling NO_x emissions. The catalyst is the core of the NH_3 -SCR reaction. Currently, the V_2O_5 - TiO_2 catalyst, which is dominant in the industry, exists some shortcomings, such as high cost, high SO_2 oxidation activity, narrow de- NO_x temperature window, and nonetheless the toxicity (Han et al., 2019a). Therefore, it is of great significance to develop novel low-cost SCR catalyst with good de- NO_x performance, low SO_2 oxidation activity, wide application temperature window, and low environmental toxicity.

Red mud (RM) is produced in alumina production. It has been proved to be active for SCR reaction to remove NO_x as a catalyst. RM is mainly consisting of Fe_2O_3 , Al_2O_3 , SiO_2 , TiO_2 , Na_2O , and etc. Among them, Fe_2O_3 has been investigated for SCR reaction because of its good catalytic activity, high N_2 selectivity, and excellent thermal stability. Meanwhile, Al_2O_3 , SiO_2 , and TiO_2 are commonly used as support materials, which could provide a porous framework for the catalyst (Lyu et al., 2021). However, Na_2O and other alkaline earth metals will sinter and block the pores of the catalyst, which is not conducive to SCR reaction. Therefore, removing alkaline substances, including free alkali and combined alkali, should be critical for the activation of RM for SCR reaction. The multi-round washing with H_2O can remove free alkali, but this process will leave the combined alkali which is difficult to dissolve in water. Acid pretreatment is an efficient approach to remove bound alkali, however, it usually comes with disadvantage of affecting the content and chemical state of other substances (Meng et al., 2021). Thus, the precise regulation of acid pretreatment is critical to optimizing the SCR activity of RM. The metal oxides and hydroxides in RM have different solubility in acid solutions. By controlling the pH during the acid pretreatment, the content and chemical state of different ions can be facilely tuned (Qiu et al., 2021). For example, different ions would dissolve into metal complexes or metal ions and interact with each other in an acidic environment. The interactions between these complexes and ions would determine the structure and chemical state of active metal in RM catalyst, thus affecting the SCR activity. Generally, the construction of a bimetallic oxide structure is generally considered to be an effective way to improve the performance of the catalyst (Zhang et al., 2012; Wang et al., 2020). Therefore, in order to enhance favorable interactions and reduce unexpected structure in RM, it is critical to precisely tuning the acid pretreatment process, which would directionally control the active sites, crystal phases, exposed planes, and etc.

In this study, we pretreated a series of Ce-modified RM (CRM) catalysts, which performed promising SCR activity

in our previous study, with different end-point of diluted HNO_3 titration (Wu et al., 2018; Gong et al., 2020). Effects from different acid pretreatment processes were discussed based on experiments and theoretical calculation. Moreover, the modification mechanism was probed.

2 Materials and methods

2.1 Catalyst preparation

The CRM-A catalysts were prepared by acid pretreatment and impregnation methods successively with dilute nitric acid (HNO_3 , analysis pure, Kermel, China) and cerium nitrate ($\text{Ce}(\text{NO}_3)_3 \cdot 6\text{H}_2\text{O}$, analysis pure, Kermel, China) as raw materials. A certain amount of original red mud was dried at 105°C for 12 h, and then ground into red mud powder (RM) with particle size less than 100 mesh (less than $150\ \mu\text{m}$). The above amount of RM was mixed with deionized water, and then titrated with 0.5 mol/L HNO_3 solution. The reaction endpoint was controlled at $\text{pH} = 3$ –5. Heated in 80°C water bath, magnetic stirring 1 h. The suspensions were denoted by RM-A, where A (3, 4, 5) was the pH value. Then, the suspensions were filtered, washed and dried (105°C , 12 h).

A certain amount of 100 mesh RM-A catalysts was mixed with deionized water, then adding Ce precursor (the dosage was calculated as $n(\text{Ce})/n(\text{Fe}_2\text{O}_3 \text{ content in RM-A}) = 1/3$, and Fe_2O_3 content in RM-A were shown in Table S1), and stirred in 80°C water bath temperature until the water was completely evaporated. Finally, a series of CRM-A catalysts were obtained by drying (105°C , 12 h) and calcination (air atmosphere, $5^\circ\text{C}/\text{min}$ heating rate, 550°C , 5 h). The CRM-W catalyst prepared by water washing without nitric acid pretreatment and calcination was used as blank control.

2.2 Catalyst characterization

The SmartLab 3KW (Rigaku, Japan) X-ray diffractometer (XRD) obtained the CRM-A catalysts crystal phase structure. The ASAP2020 (Micromeritics, USA) surface areas and porosity analyzer was used to measured and calculated the Brunauer-Emmett-Teller (BET) surface area and the average pore size of the samples. The Nicolet iS50 (Thermo Fisher, USA) was implemented to obtain the Fourier transform infrared spectroscopy (FT-IR) of the poisoned CRM-3 catalyst. The inductively coupled plasma-optical emission spectroscopy (ICP-OES) was performed on the AGILENT 720 (Agilent, China) to analyze the various elements changes in the RM during the dealcalization process. At the same time, the catalysts' chemical compositions were determined by Axios FAST (Panalytical, the Netherlands) X-ray Fluorescence (XRF) spectrometer. For collecting the X-ray photoelectron spectra (XPS), the Thermo ESCALAB 250 (Thermo

Fisher, USA) X-ray photoelectron spectrometer was implemented. The TP-5080 (Xianquan, China) temperature-programmed desorption instrument recorded the NH_3 desorption curves on the catalysts. In order to get the H_2 temperature-programmed reduction (H_2 -TPR) results, the Auto Chem II 2920 (Micromeritics, USA) chemical adsorption analyzer was used.

2.3 Catalyst activity measurement

The catalysts were tested for NH_3 -SCR de- NO_x efficiency in a fixed-bed quartz tube reactor. The reaction conditions were as follows: 4 mL catalyst, 0.05% NO , 0.05% NH_3 , 4% O_2 . The total gas flow rate was 2000 mL/min, and the gas hourly space velocity (GHSV) was 30000/h (under ambient conditions). All gases were mixed in the mixing chamber first, and then preheated to participate in the reaction. The concentration of outlet gases was monitored by the flue gas analyzer (MRU MGA5, York, Germany). The related data were collected and recorded after the SCR reaction reached a steady-state condition. The NO_x conversion (η) and the pseudo-first-order rate constant (τ , mL/(g·s)) of the SCR catalyst were calculated as followed (Eqs. (1) and (2)):

$$\eta = \frac{[\text{NO}_x]_{\text{in}} - [\text{NO}_x]_{\text{out}}}{[\text{NO}_x]_{\text{in}}} \times 100\%, \quad (1)$$

$$\tau = -\frac{V}{m} \times \ln(1 - \eta), \quad (2)$$

where $[\text{NO}_x] = \text{NO} + \text{NO}_2$, $[\text{NO}_x]_{\text{in}}$, and $[\text{NO}_x]_{\text{out}}$ are the NO_x concentration at the inlet and outlet, respectively, V is the total flow (mL/s), m is the catalyst mass (g).

2.4 DFT calculation

Compared with α - Fe_2O_3 , the RM after acid pretreatment had Al doping. To explore the Al doping effect on the NO_x conversion, the α - Fe_2O_3 and Al- Fe_2O_3 of the hexagonal structure were studied. The SCR reaction species was adsorbed on α - Fe_2O_3 (001) planes, and the Fe-O₃-Fe termination was the most stable (Liu et al., 2017b; Lyu et al., 2020). The α - Fe_2O_3 (001) model was shown in Fig. 1(a). For Al- Fe_2O_3 (001) model, it was replaced one Fe atom at the M position (shown in Fig. 1(b)) from the α - Fe_2O_3 (001) model by Al atom. The first-principle density functional theory calculations (including structural and electronic investigations), were performed based on the Cambridge Sequential Total Energy Package (CASTEP). The general gradient approximation (GGA) in the form of the Perdew-Burke-Ernzerhof (PBE) functional was adopted to treat the exchange-correlation with a plane wave cutoff of 400 eV. A force tolerance of 0.05 eV/Å, self-consistent field (SCF) of 2.0×10^{-6} eV per atom and maximum displacement of 2.0×10^{-3} Å were considered. Each atom in the storage models was allowed to relax to the minimum in the enthalpy without any constraints. The vacuum space along the z direction was set to be 15 Å, which was enough to avoid interaction between the two neighboring images. The E_{ad} according to the following

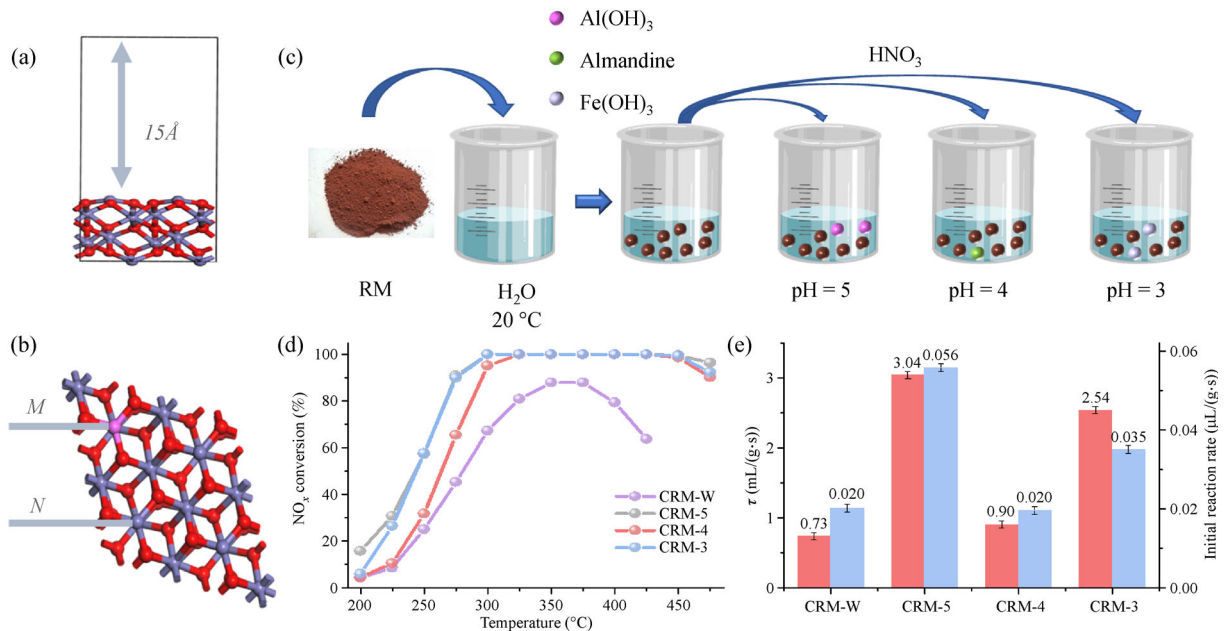


Fig. 1 (a), (b) The α - Fe_2O_3 (001) model (while the M is purple, it is Al- Fe_2O_3 (001)). The iron atoms are gray, the aluminum atoms are purple, and the oxygen atoms are red. (c) Schematic diagram of catalysts preparation. (d) The catalysts De- NO_x efficiency. (e) Reaction rate per specific surface area calculated at 225°C. Reaction conditions: $[\text{NH}_3] = [\text{NO}] = 0.05\%$, $[\text{O}_2] = 4\%$, and balanced N_2 , total flow = 2000 mL/min, gas hourly space velocity (GHSV) = 30000/h.

formula (Eq. (3)):

$$E_{ad} = E_A + E_B - E_{A+B}, \quad (3)$$

where E_A , E_B , and E_{A+B} are the energies for substrate, adsorbate, and adsorption reaction, respectively.

3 Results and discussion

3.1 NH₃-SCR performance

The schematic diagram of catalysts preparation was shown in Fig. 1(c). Figure 1(d) showed the differences in NO_x conversion between catalysts obtained by different acid pretreatment (dealkalization) processes under a gas hourly space velocity (GHSV) of 30000/h. Acid pretreated catalysts (CRM-3, CRM-4, and CRM-5) showed higher SCR activity than water washing treatment catalyst (CRM-W): nearly 100% of NO_x conversion was acquired for acid pretreated catalysts at 325°C, CRM-W catalyst yielded only 78% of NO_x conversion. Additionally, among the three acid pretreated catalysts, CRM-5 exhibited the highest NO_x conversion, followed by CRM-3, while CRM-4 showed significantly lower NO_x conversion. Figure 1(e) calculated the pseudo first order rate (τ ,

mL/(g·s)) and the initial reaction rate (k , mL/(m·s)) of the catalysts. The CRM-5 exhibited the highest τ and k , 3.04 mL/(g·s) and 0.056 mL/(m·s), respectively. The CRM-4 exhibited the lower τ and the k was as small as the CRM-W. This indicated that the decrease of active sites on the CRM-4 was the main reason for the low NO_x conversion below 300°C. However, active sites of CRM-4 showed higher activity than those on the CRM-W (Wang et al., 2021). These results suggested that the chemical state of active sites can be controlled by adjusting the acid pretreatment process, and finally the SCR activity of red mud can be improved.

3.2 Surface microstructure

The XRD patterns of the CRM-A catalysts were presented in Fig. 2(a). For CRM-W, the main crystalline phases were α -Fe₂O₃, anatase titanium dioxide, and silicate. No diffraction peaks of other components were detected, indicating that other elements existed as amorphous phases or crystalline phases with tiny particle size on the surface of CRM-W (Jiang et al., 2015). When acid pretreatment was carried out and the pH value of red mud was 5 (CRM-5), the main crystalline phases were α -Fe₂O₃ and anatase titanium dioxide. It was concluded that almost all of the

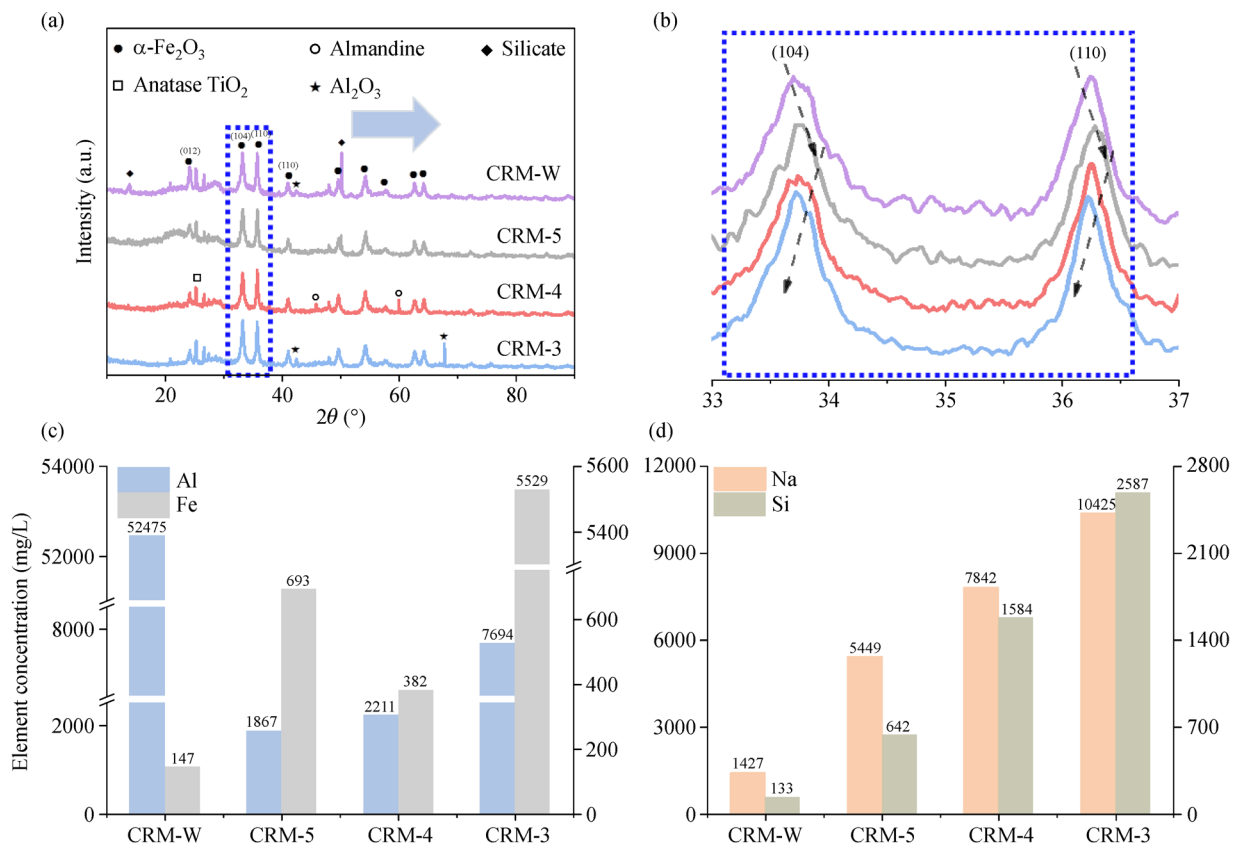


Fig. 2 (a), (b) XRD spectra, and (c), (d) element composition of the supernatant of the acid-leached sample detected by ICP-OES experiments.

crystalline silicate vanished. When adding acid continuously until pH = 4 (CRM-4), the diffraction peaks of almandine appeared, which may be due to the complete dissolution of aluminosilicate, and the substitution reaction between iron ion and aluminum ion generated aluminobutyric acid. For CRM-3, the diffraction peaks of almandine disappeared, and that of alumina appeared at the same time. Figure 2(b) showed the part of $\alpha\text{-Fe}_2\text{O}_3$ diffraction peaks of CRM-A catalysts. Compared with the CRM-W, the diffraction peaks of $\alpha\text{-Fe}_2\text{O}_3$ of the CRM-5 slightly shifted to a higher angle. While the corresponding diffraction peaks of CRM-4 and CRM-3 moved to lower angle relative to CRM-5. The former indicated that some ions with a radius smaller than Fe^{3+} (such as Na^+ , Al^{3+}) dissolve and dope into $\alpha\text{-Fe}_2\text{O}_3$ lattice, resulting in the decrease of $\alpha\text{-Fe}_2\text{O}_3$ lattice parameters. The latter suggested that as the amount of acid increased, impurity ions were precipitated with the dissolution of Fe^{3+} .

The crystallite parameters of main crystal planes of $\alpha\text{-Fe}_2\text{O}_3$ phase were listed in Table 1. The results showed that the pH value affected the crystal size and crystallinity of $\alpha\text{-Fe}_2\text{O}_3$. Compared with the CRM-W, the full width at half maximum (FWHM) increased, and the crystallite sizes were markedly decreased for the CRM-5 and CRM-3. However, the change law of FWHM and crystallite sizes in CRM-4 was opposite to that of CRM-5 and CRM-3. The decrease of the grain size of $\alpha\text{-Fe}_2\text{O}_3$ indicated that the dispersion of $\alpha\text{-Fe}_2\text{O}_3$ on the catalyst surface was improved, which was beneficial to enhance the NO_x conversion (Gao et al., 2017; Liu et al., 2017a).

Figure S1 showed the SEM of CRM-A catalysts. The influence of different acid pretreatment processes on the microstructure of the catalyst was studied. With the decrease of pH value, the catalyst particles presented a certain dispersion and the cluster phenomenon weakened. This showed that the removal of silicate components was conducive to reducing the diffusion resistance of SCR reactants in the catalyst. Figure S2 displayed pore size

distribution curves of the CRM-A catalysts. Compared with CRM-W catalyst, all acid pretreated catalysts exhibited more abundant pore structure. In particular, CRM-3 presented a sharp peak at about 3 nm, and CRM-5 showed a broad pore size distribution in the range of 2–30 nm. Micropores provide a large specific surface and pore volume improving the acid sites (Hu et al., 2015; Ma et al., 2020), while mesopores facilitate surface adsorption of reactants and reductants on the catalyst, ensuring mass and diffusion (Liu and Ihl Woo, 2006). Both were beneficial to improve catalytic activity. All isotherms were similar to the type-II isotherm according to the IUPAC classification (Fig. S3). The hysteresis loops exhibited a shape of typical H3 type, revealing the existence of the slit-shaped pore structures in these catalysts.

The BET surface area, specific pore volume, and average pore size were summarized in Table 2. The surface area and specific pore volume of the catalysts increased significantly, and the average pore diameter decreased slightly after acid pretreatment (Liu et al., 2020). This is because that compared with water washing treatment, acid pretreatment could remove alkaline compounds that are insoluble in water but soluble in acid. Also, acid pretreatment could reduce the content of some metal ions that can promote particle agglomeration. These changes in physical properties enhanced the interpore connectivity, contributed to providing more active adsorption sites for SCR reaction and reducing the diffusion resistance of SCR reactants in the catalyst. However, due to almandine deposited on the surface of the CRM-4 catalyst covered the active centers and blocked the catalyst channels, the specific surface area of CRM-4 was lower than that of CRM-5 and CRM-3.

Figures 2(c) and 2(d) showed the concentrations of some elemental ions in CRM-A suspensions. With the process of acid pretreatment, the physical and chemical properties of each ion and the interaction between different ions changed. For Al element, the aqueous solution of the CRM-W was alkaline, and Al_2O_3 reacted with OH^- at this time: $\text{Al}_2\text{O}_3 +$

Table 1 Different crystallite parameters of CRM-A catalysts by XRD results

Catalysts	(104) plane		(110) plane	
	FWHM (°)	D (nm)	FWHM (°)	D (nm)
CRM-W	0.531	15.44	0.369	22.37
CRM-5	0.552	14.85	0.386	21.38
CRM-4	0.511	16.04	0.405	20.38
CRM-3	0.554	14.80	0.422	19.56

Table 2 Surface physical properties of the CRM-A catalysts by BET results

Samples	BET surface area (m^2/g)	Specific pore volume (cm^3/g)	Average pore size (nm)
CRM-W	36.37	0.159	17.46
CRM-5	54.56	0.187	13.79
CRM-4	46.14	0.168	14.56
CRM-3	72.42	0.179	9.91

$2\text{OH}^- \rightarrow 2\text{AlO}_2^- + \text{H}_2\text{O}$. Al ions in CRM-5 were mainly adsorbed on RM as $\text{Al}(\text{OH})_3$ colloidal body, resulting in less free Al ions. For CRM-4 and CRM-3 samples, the reactions related to aluminum element were $\text{Al}_2\text{O}_3 + 6\text{H}^+ \rightarrow 2\text{Al}^{3+} + 3\text{H}_2\text{O}$ and $\text{Al}(\text{OH})_3 + 3\text{H}^+ \rightarrow \text{Al}^{3+} + 3\text{H}_2\text{O}$. Besides, with the increase of H^+ concentration, the concentration of Fe^{3+} first increased, then decreased and then increased again. This may be because the Fe^{3+} which had been dissolved and dissociated before would react with silicon and aluminum compounds to generate almandine when $\text{pH} = 4$, reducing the content of free Fe^{3+} . When $\text{pH} = 3$, almandine would be dissolved, and made Fe^{3+} dissociated. These results were consistent with XRD results. Due to Na ions located in the RM channel and skeleton were insoluble in water, the content of free Na ions in CRM-W was very low. After acid pretreatment, it was found that the more acid used, the more free Na ions content. The change of Si with acid content was the same as that of Na, indicating that acid pretreatment was an effective approach to remove bound alkali.

3.3 The chemical state of surface composition

XPS spectra were employed to reveal the compositional and chemical states of the three acid pretreated catalysts. The Fe 2p spectra of the catalysts were illustrated in Fig. 3(a). The characteristic peaks of 710.5 and 724.8 eV could be attributed to Fe 2p_{3/2} and Fe 2p_{1/2}, respectively. By performing a peak fitting deconvolution, the Fe 2p_{3/2} could be separated into two peaks, the peaks at 712 and 711.9 eV correspond to Fe^{3+} and that of 710.1, 710.2, and 710.3 eV correspond to Fe^{2+} , respectively. The peaks at 724.6 and 724.8 eV of Fe 2p_{1/2} and the satellite peaks at 718.8 and 719.4 eV were typical for Fe^{3+} . These results indicated that the Fe^{3+} and Fe^{2+} existed simultaneously on these catalysts. Compared with CRM-4, the Fe^{3+} binding energy of CRM-5 and CRM-3 slightly increased. The higher binding energy indicated that the outer electron cloud density near Fe^{3+} decreased. The reduction of electron cloud density increased the electronegativity of Fe^{3+} , which was beneficial to improve SCR activity (Zhao et al., 2013). The relative percentages of Fe^{2+} and Fe^{3+} were shown in Table 3. The ratio of Fe^{3+} calculated by $\text{Fe}^{3+} / (\text{Fe}^{2+} + \text{Fe}^{3+})$ were about 79.16% and 81.46% for CRM-5 and CRM-3, respectively, whereas the ratio was about 69.68% on the CRM-4. The high ratio of Fe^{3+} proved that the high average oxidation state is the key to adsorb NH_3 , which is conducive to the SCR reaction.

The Ce 3d XPS spectra of CRM-A catalysts were displayed in Fig. 3(b). The peaks at 882.2–889.2 eV and 900.8–916.7 eV was attributed to Ce 3d_{5/2} and Ce 3d_{3/2}, respectively. The peaks around 882.2, 889, 898.3, 900.8, 907.7, and 916.7 eV belonged to Ce^{4+} species, while the other peaks correspond to Ce^{3+} species. The relative content of Ce^{3+} in CRM-5, CRM-4 and CRM-3 were 43.12%, 29.84% and 40.02%, respectively. Ce^{3+} had a

positive effect on catalytic activity because it can generate more oxygen vacancies, which would promote NH_3 adsorption (Zha et al., 2017). Also, Ce^{3+} could speed up the NO to NO_2 process, thereby increasing the low-temperature activity (Yi et al., 2019). Therefore, CRM-5 and CRM-3 showed better SCR activity at 200°C–450°C. The O 1s XPS spectra of CRM-A catalysts were displayed in Fig. 3(c). The O 1s peaks can be fitted into two peaks, which indicated that the CRM-A catalysts possessed two kinds of oxygen. Peaks around 531.6 eV (denoted as O_α) were attributed to the adsorbed oxygen, corresponding to the O_2^{2-} caused by the surface oxygen defect, or the O^- corresponding to $-\text{OH}$, and the peak around 529.8 eV (denoted as O_β) represented lattice oxygen (Wang et al., 2018). The surface contents of O_α and O_β were displayed in Table S2, and the $\text{O}_\alpha / (\text{O}_\alpha + \text{O}_\beta)$ ratio of CRM-5, CRM-4, and CRM-3 were 13.58%, 16.39% and 20.67%, respectively. The results showed that the increased acid amount could increase the surface chemically adsorbed oxygen. Based on all the XPS characterization data, we concluded that O_α contributed less to the reaction than Lewis acid sites of Fe ion sites and oxygen vacancy with coordinatively unsaturated Ce^{3+} . Therefore, the surface chemically adsorbed oxygen was not the main factor affecting the SCR activity.

3.4 Redox and surface acidity behavior

The NH_3 -TPD evaluated the overall acidic properties of the three acid pretreated catalysts. As shown in Fig. 4(a), all NH_3 -TPD profiles presented two desorption peaks. Compared with NH_3 molecules adsorbed on Lewis acid sites, NH_4^+ ions adsorbed on Brønsted acid sites had lower thermal stability (Han et al., 2019b). The desorption peaks at 200°C–300°C resulted from the NH_3 desorption at Brønsted acid sites, whereas NH_3 desorption at Lewis acid sites formed the desorption peaks at 350°C–550°C (Wang et al., 2016; Zhang et al., 2020). The peaks of 225°C and 256°C corresponded to Brønsted acid sites; 434°C, 449°C, and 454°C corresponded to Lewis acid sites. As known, the peak area was proportional to the number of acid sites on the catalysts, and catalysts with more acid sites tended to have better performance. As can be seen from Fig. 4(a), the CRM-5 had the largest amount of acid sites, especially the amount of Brønsted acid, which was consistent with the SCR activity results. For the CRM-4 and CRM-3, there was no significant difference in the overall acid amount between them, and even the amount of Lewis acid at $\text{pH} = 4$ was more than that at $\text{pH} = 3$, which may indicate that the contribution of Brønsted acid sites was significantly greater than that of Lewis acid sites in the SCR reaction process. In addition, compared with CRM-3, the two NH_3 desorption peaks of CRM-4 moved to higher temperature, which was another important factor that contributed to its lower SCR activity.

The H_2 -TPR experiments were carried out to investigate

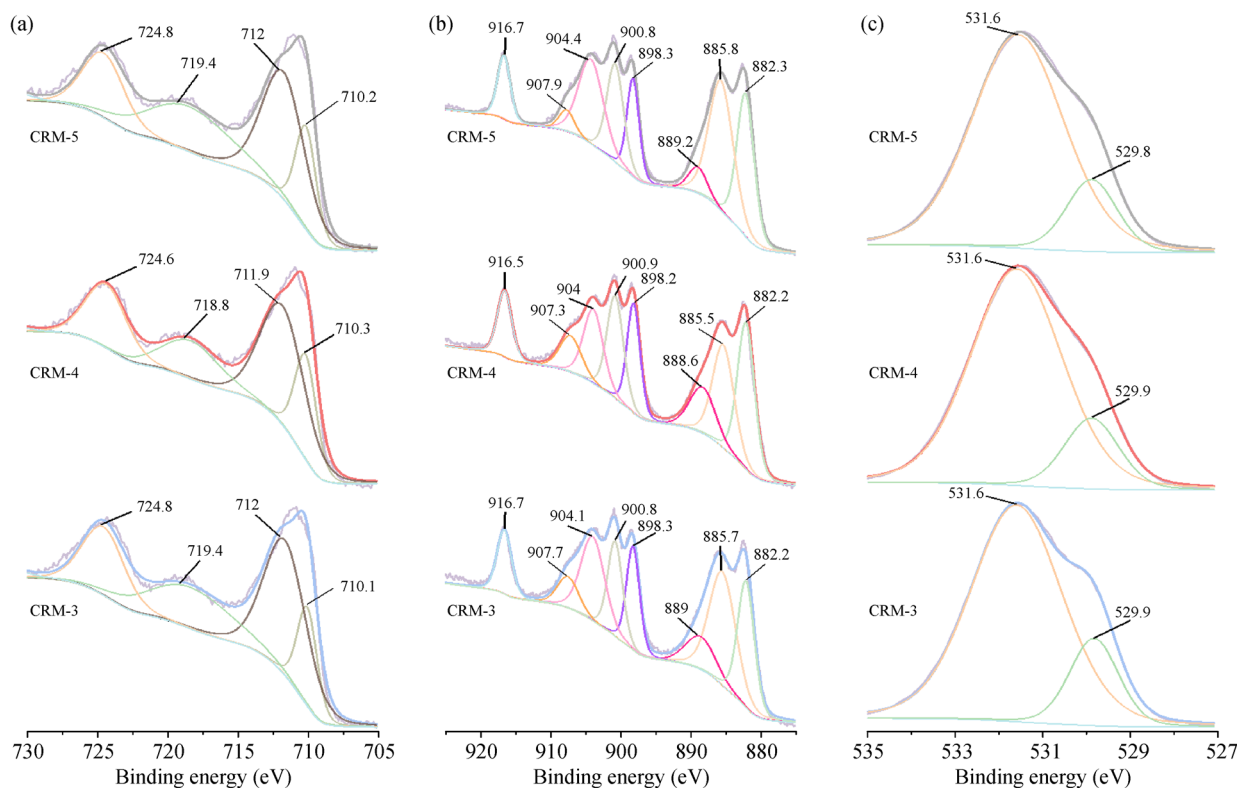


Fig. 3 XPS spectra of the CRM-5, CRM-4, and CRM-3 catalysts over the spectral regions of (a) Fe 2p, (b) Ce 3d, and (c) O 1s.

Table 3 Surface chemical properties of the CRM-A catalysts by XPS results

Catalysts	Relative atomic ratio (%)				Surface atomic concentration (%)	
	Fe 2p		Ce 3d		Fe 2p	
	Fe ³⁺	Fe ²⁺	Ce ⁴⁺	Ce ³⁺	Fe ³⁺	Fe ²⁺
CRM-5	79.16	20.84	56.88	43.12	18.64	4.91
CRM-4	69.68	30.32	70.16	29.84	18.47	8.04
CRM-3	81.46	18.54	59.98	40.02	23.84	5.42

the effect of Fe species on the redox properties of the CRM-A catalysts, and the results were shown in Fig. 4(b). The reduction peaks appeared at about 500°C and 700°C were attributed to the reduction process of $\text{Fe}_2\text{O}_3 \rightarrow \text{FeO}$ and $\text{FeO} \rightarrow \text{Fe}$, respectively (Liu et al., 2018; Chen et al., 2021). The peaks slightly shifted toward higher temperature for CRM-5 and CRM-3, compared with CRM-W and CRM-4. This demonstrated that iron oxides in CRM-5 and CRM-3 catalysts were less easily reduced. For one thing, the existence of Fe-O-Al bond, which were formed by the interaction between Fe and Al, strengthened the Fe-O-Fe bond. And the strong interaction between the stoichiometric Ce and O ($\text{Ce}^{4+}\text{-O-Ce}^{4+}$) as well as the interaction between the non-stoichiometric Ce and O ($\text{Ce}^{3+}\text{-O-Ce}^{4+}$) provided the CRM-5 and CRM-3 catalysts with more oxygen vacancies. The increase of oxygen vacancies also reduced the reducibility of the catalysts (Zhang et al.,

2015; Jia et al., 2020). Figure 4(c) showed the practical H_2 consumption of the CRM-A catalysts. The acid pretreatment process removed the agglomerated metal salts and released the Fe^{3+} active species, which increased the H_2 consumption of the catalysts. It can be seen that the H_2 consumption of both CRM-5 and CRM-3 were significantly higher than that of CRM-W, while the H_2 consumption of CRM-4 was only slightly increased. This is because most Fe^{3+} of CRM-4 catalyst generated into almandine but was not released, which was not conducive to the REDOX cycle in NH_3 -SCR reaction (Guo et al., 2017).

3.5 Anti-poisoning test

Figure 5(a) showed the influences of H_2O and SO_2 on the CRM-5 catalyst at 300°C. Only 9% of NO conversion was

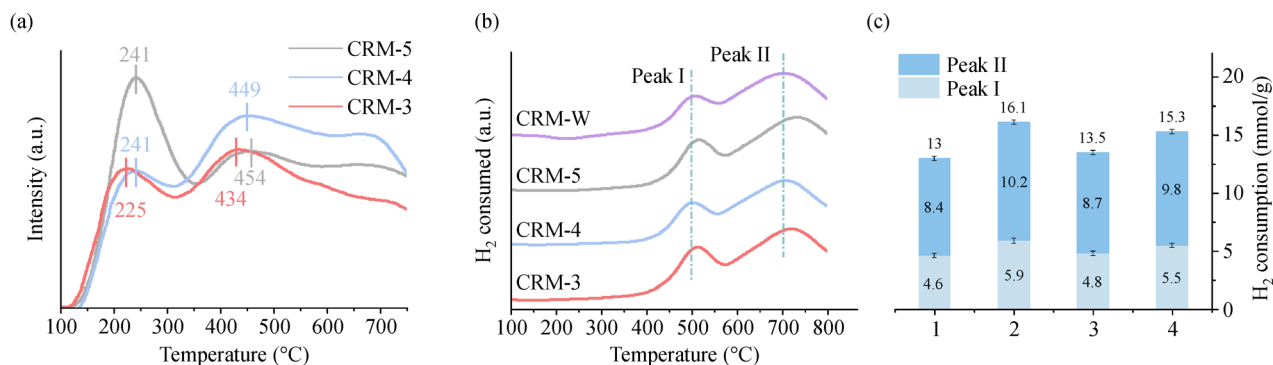


Fig. 4 (a) NH₃-TPD profiles of the CRM-5, CRM-4, and CRM-3 catalysts, (b) H₂-TPR profiles of the catalysts, and (c) H₂ consumption.

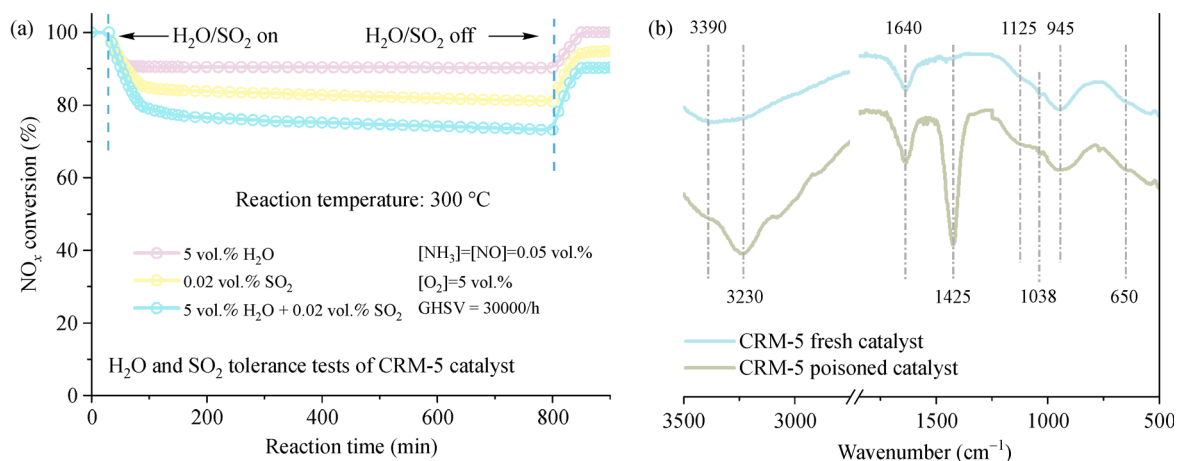


Fig. 5 (a) H₂O and SO₂ effect on NO_x conversion over the CRM-5 catalyst, (b) FT-IR spectra of fresh and poisoned CRM-5 catalyst.

lost when H₂O was introduced, and part of the catalytic activity was recovered after its removal. In contrast, nearly 20% of NO conversion was lost with the introduction of SO₂, and the NO_x conversion recovered to 93% upon the removal of SO₂. When H₂O and SO₂ were added together to the system, the NO_x conversion decreased significantly, slowly decreasing from 100% to 71%. When both were removed, the NO_x conversion only recovered to 90%. Figure 5(b) recorded the FT-IR spectra of used CRM-5 catalyst in the presence or absence of SO₂ and H₂O. The peaks at 3390, 3230, and 1640 cm⁻¹ corresponded to the O-H tensile vibration peaks of chemisorbed water and -OH groups. The bands at 1425 cm⁻¹ belonged to asymmetrical vibrations of NH₄⁺ at the Brønsted acid sites, while peaks at 945, 1038 and 1125 cm⁻¹ were attributed to the sulfate species. Compared with the CRM-5 fresh catalyst, the CRM-5 poisoned catalyst had a significant NH₄⁺ absorption peak and weak SO₄²⁻ absorption peaks. This indicated that NH₄⁺ and SO₄²⁻ deposited on the surface of the catalyst when H₂O and SO₂ were introduced, resulting in a decrease in the number of active sites and reducing the NO_x conversion.

The above results indicated that when H₂O was intro-

duced, it would produce competitive adsorption with NH₃. This reduced the activity, but the effect was reversible. Compared with H₂O, SO₂ had an adverse influence on the CRM-5 catalyst, and the effect was irreversible. There are two reasons: 1) SO₂ reacted with the reactants (NH₃ and O₂) to produce hard-to-decompose ammonium sulfate. Ammonium sulfate would deposit on the surface of the catalyst, reducing the number of active sites and leading to reduction of NO_x conversion (Lee and Bai, 2018); 2) SO₂ could react with metal oxides to form metal sulfates, resulting in the catalyst deactivation.

3.6 Theoretical calculation

The influence of Al doping for Fe-based catalyst on the adsorption reaction gas (NH₃, NO) was calculated by DFT method. The calculation was carried out on the non-stoichiometric Fe₂O₃ surfaces to ensure the calculation results reliable. The optimized adsorption model of NO and NH₃ on α-Fe₂O₃ (001) and Al-Fe₂O₃ (001) surfaces were shown in Fig. 6. The atomic distance and E_{ad} of each stable model after optimization were listed in Table 4. The results showed that the distance between N and Fe and E_{ad}

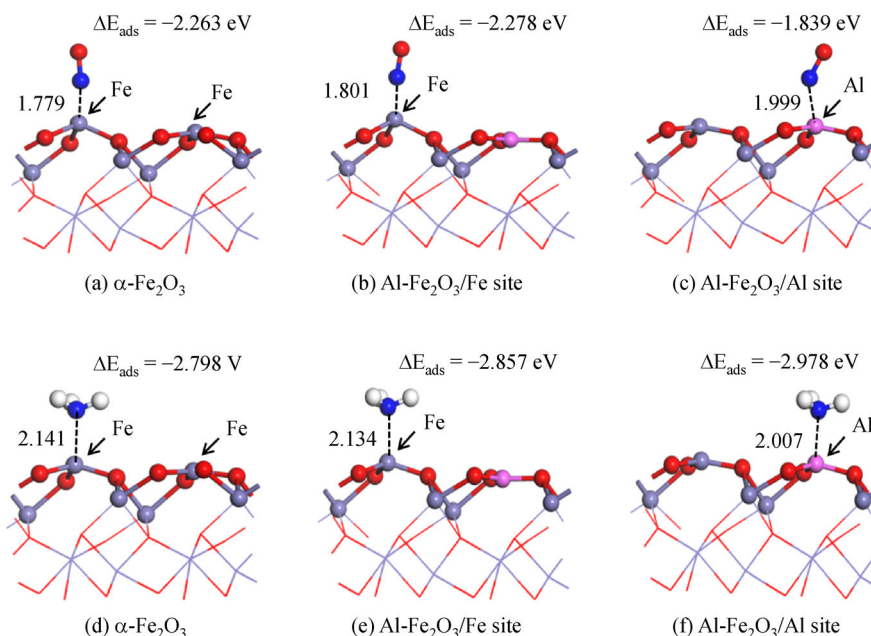


Fig. 6 Optimized adsorption model of the NO on (a) α -Fe₂O₃(001), (b) and (c) Al-Fe₂O₃ (001) surfaces; optimized adsorption model of the NH₃ on (d) α -Fe₂O₃ (001), (e) and (f) Al-Fe₂O₃ (001) surfaces. The iron atoms are gray, the aluminum atoms are purple, the oxygen atoms are red, and the hydrogen atoms are white.

Table 4 The optimal distance and E_{ad} for models to adsorb NO and NH₃

Gas	Model	Adsorption site	Atomic distance (Å)	E_{ad} (eV)
NO	α -Fe ₂ O ₃ (001)	Fe	1.779	-2.263
	Al-Fe ₂ O ₃ (001)	Al	1.999	-1.839
	Al-Fe ₂ O ₃ (001)	Fe	1.801	-2.278
NH ₃	α -Fe ₂ O ₃ (001)	Fe	2.141	-2.798
	Al-Fe ₂ O ₃ (001)	Al	2.007	-2.978
	Al-Fe ₂ O ₃ (001)	Fe	2.134	-2.857

of NO adsorption on Fe₂O₃ (001) were 1.779 Å and -2.263 eV, respectively. The interatomic distances of NO adsorption on Al-Fe₂O₃ (001) were 1.999 Å (adsorbed on Al site) and 1.801 Å (adsorbed on Fe site), and the E_{ad} were -1.839 eV (adsorbed on Al site) and -2.278 eV (adsorbed on Fe site). The NO was more tend to adsorb on Fe sites of Al-Fe₂O₃ (001), which indicated that Al doping was beneficial to NO adsorption on Fe₂O₃. The E_{ad} of NH₃ on Fe₂O₃ (001) model was -2.798 eV, and that of NH₃ on Al-Fe₂O₃ (001) model were -2.857 eV (adsorbed on Fe site) and -2.978 eV (adsorbed on Al site), respectively. These indicated that NH₃ more easily adsorbe on the Al site of Al-Fe₂O₃ (001), and the adsorption is more stable. DFT results showed that the adsorption capacity of the Al-O₃-Fe for NH₃ and NO is stronger than that of Fe-O₃-Fe, which enhanced the NO_x conversion of the catalyst.

Combined with XRD and ICP characterization, it can be

found that Al ions were in a free state for CRM-5. Part of Al ions would enter Fe₂O₃, resulting in enhanced interaction between Al and Fe₂O₃, which improved the adsorption capacity of the catalyst for NH₃ and NO. When pH = 4, some Al ions combined with free Fe ions and Si ions to form inactive substance almandine. The interaction between Al and Fe₂O₃ was weakened and the adsorption of NH₃ and NO was suppressed. When pH = 3, the almandine dissolved and the iron oxide formed colloid to adsorb free Al ions, which was beneficial to the interaction between them.

4 Conclusions

In this paper, the content of acid in red mud catalyst was controlled by adjusting the pH value of the titration endpoint, so as to research the effects of different acid

pretreatment (dealkalization) processes on the acidity and reducibility of red mud. Acid pretreated catalysts (CRM-3, CRM-4, and CRM-5) showed higher SCR activity than water washing treatment catalyst (CRM-W): nearly 100% of NO_x conversion was acquired for acid pretreated catalysts at 325°C, CRM-W catalyst yielded only 78% of NO_x conversion. Additionally, among the three acid pretreated catalysts, CRM-5 exhibited the highest NO_x conversion, followed by CRM-3, while CRM-4 showed significantly lower NO_x conversion. Good pore structure, high initial reaction rate, high Fe³⁺/(Fe³⁺ + Fe²⁺) and Ce³⁺/(Ce³⁺ + Ce⁴⁺) ratio, strong surface acidity, much H₂ consumption and strong interaction between Fe and Al were the reasons for the excellent NH₃-SCR performance of CRM-5 and CRM-3 catalysts. The results of DFT indicated that the adsorption capacity of Al-O₃-Fe on NH₃ and NO was stronger than that of Fe-O₃-Fe, which improved the NO_x conversion of the catalyst. However, for CRM-4 catalyst, most of Fe³⁺ and Al³⁺ formed almandine but were not released, which weakened the interaction between Al and Fe. Also, almandine deposited on the catalyst surface covered the active sites, resulting in poor NH₃-SCR activity.

Acknowledgements This work was financially supported by the National Natural Science Foundation of China (Grant No. 21906090), the National Key Research and Development Program of China (Nos. 2017YFC0210200 and 2017YFC0212800), and the Primary Research & Development Project of Shandong Province (China) (Nos. 2018GSF117034 and 2019JZZY020305). The scientific calculations in this paper have been done on the HPC Cloud Platform of Shandong University (China).

Electronic Supplementary Material Supplementary material is available in the online version of this article at <https://doi.org/10.1007/s11783-021-1447-x> and is accessible for authorized users.

References

- Chen Q Z, Zhang X, Li B, Niu S L, Zhao G J, Wang D, Peng Y, Li J H, Lu C M, Crittenden J (2021). Insight into the promotion mechanism of activated carbon on the monolithic honeycomb red mud catalyst for selective catalytic reduction of NO_x. *Frontiers of Environmental Science & Engineering*, 15(5): 92
- Gao F Y, Tang X L, Yi H H, Li J Y, Zhao S Z, Wang J G, Chu C, Li C L (2017). Promotional mechanisms of activity and SO₂ tolerance of Co- or Ni-doped MnO_x-CeO₂ catalysts for SCR of NO_x with NH₃ at low temperature. *Chemical Engineering Journal*, 317: 20–31
- Gong Z Q, Ma J, Wang D, Niu S L, Yan B H, Shi Q L, Lu C M, Crittenden J (2020). Insights into modified red mud for the selective catalytic reduction of NO_x: Activation mechanism of targeted leaching. *Journal of Hazardous Materials*, 394: 122536
- Guo R T, Li M Y, Sun P, Pan W G, Liu S M, Liu J, Sun X, Liu S W (2017). Mechanistic investigation of the promotion effect of Bi modification on the NH₃-SCR performance of Ce/TiO₂ catalyst. *Journal of Physical Chemistry C*, 121(49): 27535–27545
- Han L P, Cai S X, Gao M, Hasegawa J Y, Wang P L, Zhang J P, Shi L Y, Zhang D S (2019a). Selective catalytic reduction of NO_x with NH₃ by using novel catalysts: State of the art and future prospects. *Chemical Reviews*, 119(19): 10916–10976
- Han L P, Gao M, Feng C, Shi L Y, Zhang D S (2019b). Fe₂O₃-CeO₂@Al₂O₃ nanoarrays on Al-mesh as SO₂-tolerant monolith catalysts for NO_x reduction by NH₃. *Environmental Science & Technology*, 53(10): 5946–5956
- Hu H, Cai S X, Li H R, Huang L, Shi L Y, Zhang D S (2015). Mechanistic aspects of deNO_x processing over TiO₂ supported Co-Mn oxide catalysts: Structure-activity relationships and in situ DRIFTS analysis. *ACS Catalysis*, 5(10): 6069–6077
- Jia H Z, Shi Y F, Nie X F, Zhao S, Wang T C, Sharma V K (2020). Persistent free radicals in humin under redox conditions and their impact in transforming polycyclic aromatic hydrocarbons. *Frontiers of Environmental Science & Engineering*, 14(4): 73
- Jiang Y, Xing Z M, Wang X C, Huang S B, Wang X W, Liu Q Y (2015). Activity and characterization of a Ce-W-Ti oxide catalyst prepared by a single step sol-gel method for selective catalytic reduction of NO with NH₃. *Fuel*, 151(1): 124–129
- Lee T Y, Bai H L (2018). Metal sulfate poisoning effects over MnFe/TiO₂ for selective catalytic reduction of NO by NH₃ at low temperature. *Industrial & Engineering Chemistry Research*, 57(14): 4848–4858
- Liu J, Li G Q, Zhang Y F, Liu X Q, Wang Y, Li Y (2017a). Novel Ce-W-Sb mixed oxide catalyst for selective catalytic reduction of NO_x with NH₃. *Applied Surface Science*, 401: 7–16
- Liu J X, Liu J, Zhao Z, Tan J B, Wei Y C, Song W Y (2018). Fe/Beta@SBA-15 core-shell catalyst: Interface stable effect and propene poisoning resistance for NO abatement. *AIChE Journal*, 64(11): 3967–3978
- Liu J X, Zhao Z, Xu C M, Liu J (2019). Structure, synthesis, and catalytic properties of nanosize cerium-zirconium-based solid solutions in environmental catalysis. *Chinese Journal of Catalysis*, 40(10): 1438–1487
- Liu S, Lin Q J, Liu J Y, Xu S H, Wang Y, Xu H D, Wang J L, Chen Y Q (2020). Enhancement of the hydrothermal stability of WO₃/Ce_{0.68}Zr_{0.32}O₂ catalyst by silica modification for NH₃-SCR. *ACS Applied Energy Materials*, 3(1): 1161–1170
- Liu Z M, Ihl Woo S (2006). Recent advances in catalytic deNO_x Science and Technology. *Catalysis Reviews. Science and Engineering*, 48(1): 43–89
- Liu Z, Yu R T, Dong Y P, Li W, Lv B L (2017b). The adsorption behavior and mechanism of Cr (VI) on 3D hierarchical α-Fe₂O₃ structures exposed by (0 0 1) and non-(0 0 1) planes. *Chemical Engineering Journal*, 309: 815–823
- Lyu F, Hu Y H, Wang L, Sun W (2021). Dealkalization processes of bauxite residue: a comprehensive review. *Journal of Hazardous Materials*, 403: 123671
- Lyu Z K, Niu S L, Lu C M, Zhao G J, Gong Z Q, Zhu Y (2020). A density functional theory study on the selective catalytic reduction of NO by NH₃ reactivity of α-Fe₂O₃ (0 0 1) catalyst doped by Mn, Ti, Cr and Ni. *Fuel*, 267: 117147
- Ma S B, Tan H S, Li Y S, Wang P Q, Zhao C, Niu X Y, Zhu Y J (2020). Excellent low-temperature NH₃-SCR NO removal performance and enhanced H₂O resistance by Ce addition over the Cu_{0.02}Fe_{0.2}Ce_yTi_{1-x}O_x (y = 0.1, 0.2, 0.3) catalysts. *Chemosphere*, 243: 125309

- Meng Y, Liu W V, Fiedler H, Zhang J L, Wei X R, Liu X H, Peng M, Zhang T T (2021). Fate and risk assessment of emerging contaminants in reclaimed water production processes. *Frontiers of Environmental Science & Engineering*, 15(5): 104
- Qiu S J, Liu J J, Zhang L, Zhang Q, Peng Y Z (2021). Sludge fermentation liquid addition attained advanced nitrogen removal in low C/N ratio municipal wastewater through short-cut nitrification-denitrification and partial anammox. *Frontiers of Environmental Science & Engineering*, 15(2): 26
- Sun F W, Liu H B, Shu D B, Chen T H, Chen D (2019). The characterization and SCR performance of Mn-containing α -Fe₂O₃ derived from the decomposition of siderite. *Minerals*, 9(7): 393–404
- Wang B, Ma J, Wang D, Gong Z Q, Shi Q L, Gao C, Lu C M, Crittenden J (2021). Acid-pretreated red mud for selective catalytic reduction of NO with NH₃: Insights into inhibition mechanism of binders. *Catalysis Today*, 376: 247–254
- Wang D, Peng Y, Yang Q, Xiong S, Li J, Crittenden J (2018). Performance of modified La_xSr_{1-x}MnO₃ perovskite catalysts for NH₃ oxidation: TPD, DFT, and kinetic studies. *Environmental Science & Technology*, 52(13): 7443–7449
- Wang D, Yang Q L, Yang G P, Xiong S C, Li X S, Peng Y, Li J H, Crittenden J (2020). Rational tuning towards A/B-sites double-occupying cobalt on tri-metallic spinel: Insights into its catalytic activity on toluene catalytic oxidation. *Chemical Engineering Journal*, 399: 125792
- Wang P, Sun H, Quan X, Chen S (2016). Enhanced catalytic activity over MIL-100(Fe) loaded ceria catalysts for the selective catalytic reduction of NO_x with NH₃ at low temperature. *Journal of Hazardous Materials*, 301: 512–521
- Wu J K, Gong Z Q, Lu C M, Niu S L, Ding K, Xu L T, Zhang K (2018). Preparation and performance of modified red mud-based catalysts for selective catalytic reduction of NO_x with NH₃. *Catalysts*, 8(1): 35–50
- Yi H, Huang Y, Tang X, Zhao S, Gao F, Xie X, Wang J, Yang Z (2019). Mn-CeO_x/MeO_x(Ti, Al)/cordierite preparation with ultrasound-assisted for non-methane hydrocarbon removal from cooking oil fumes. *Ultrasonics Sonochemistry*, 53: 126–133
- Zha K W, Cai S X, Hu H, Li H R, Yan T T, Shi L Y, Zhang D S (2017). In situ DRIFTS investigation of promotional effects of tungsten on MnO_x-CeO₂/meso-TiO₂ catalysts for NO_x reduction. *Journal of Physical Chemistry C*, 121(45): 25243–25254
- Zhang H, Jin M, Xia Y (2012). Enhancing the catalytic and electrocatalytic properties of Pt-based catalysts by forming bimetallic nanocrystals with Pd. *Chemical Society Reviews*, 41(24): 8035–8049
- Zhang L, Li L L, Cao Y, Xiong Y, Wu S G, Sun J F, Tang C J, Gao F, Dong L (2015). Promotional effect of doping SnO₂ into TiO₂ over a CeO₂/TiO₂ catalyst for selective catalytic reduction of NO by NH₃. *Catalysis Science & Technology*, 5(4): 2188–2196
- Zhang Q L, Zhang Y Q, Zhang T X, Wang H M, Ma Y P, Wang J F, Ning P (2020). Influence of preparation methods on iron-tungsten composite catalyst for NH₃-SCR of NO: The active sites and reaction mechanism. *Applied Surface Science*, 503: 144190
- Zhao W, Zhong Q, Pan Y X, Zhang R (2013). Systematic effects of S-doping on the activity of V₂O₅/TiO₂ catalyst for low-temperature NH₃-SCR. *Chemical Engineering Journal*, 228(6): 815–823